

# How stable are 2H-MoS<sub>2</sub> edges under Hydrogen Evolution Reaction conditions?

Nawras Abidi,<sup>†</sup> Audrey Bonduelle-Skrzypczak,<sup>‡</sup> and Stephan N. Steinmann<sup>\*,†</sup>

<sup>†</sup>*Univ Lyon, Ens de Lyon, CNRS UMR 5182, Université Claude Bernard Lyon 1,  
Laboratoire de Chimie, F69342, Lyon, France*

<sup>‡</sup>*IFP Energies nouvelles, Rond-point de l'échangeur de Solaize, 69360 Solaize, France*

E-mail: [stephan.steinmann@ens-lyon.fr](mailto:stephan.steinmann@ens-lyon.fr)

Phone: (+33)4 72 72 81 55

## Abstract

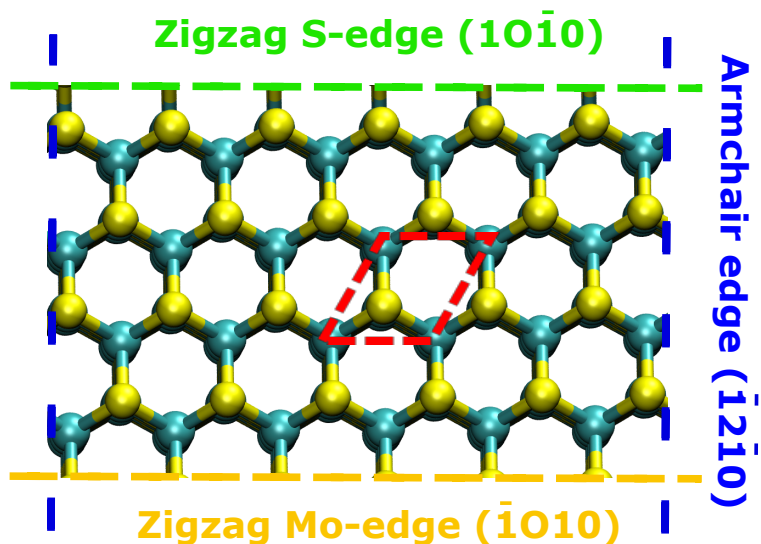
Transition metal dichalcogenides (TMDs), especially MoS<sub>2</sub>, have emerged as a promising class of electrocatalysts for the production of H<sub>2</sub> via the hydrogen evolution reaction (HER) in acidic conditions. The edges of MoS<sub>2</sub> are known for their HER activity, but their precise atomistic nature and stability under HER conditions is not yet known. In contrast to other typical uses of MoS<sub>2</sub> as a catalyst, under HER there is no external source of sulfur. Therefore, the sulfidation of the edges can only decrease under operating conditions and the thermodynamics of the process are somewhat ill-defined. Our results suggest that the 50%S S-edge may be active for HER via the Volmer-Tafel mechanism and is, despite a high H coverage, stable with respect to H<sub>2</sub>S release. At the 50%S Mo-edge, the adsorbed hydrogen opens the way for H<sub>2</sub>S release, leading to the 0%S Mo-edge, which was previously investigated and found to be HER active. HER being a water-based process, we also considered the effect of the presence of H<sub>2</sub>O and the in-situ formation of OH. For the 50%S Mo-edge, H<sub>2</sub>O is only very weakly adsorbed and OH formation is unfavorable. Nevertheless, OH assists the loss of sulfur coverage, leading to OH-based HER active sites. In contrast, OH is strongly adsorbed on the 50%S S-edge. By explicitly considering the electrochemical potential using grand-canonical density functional theory, we unveil that the Volmer-Heyrovsky mechanism on sulfur sites is still accessible in the presence of surface OH at the 50%S S-edge. However, the 50%S S-edge is found to be mildly unstable with respect to H<sub>2</sub>S in the presence of water/OH. Hence, we suggest that the 50%S S-edge evolves over time towards a 0%S S-edge, covered by surface OH that will block permanently the active sites.

## Introduction

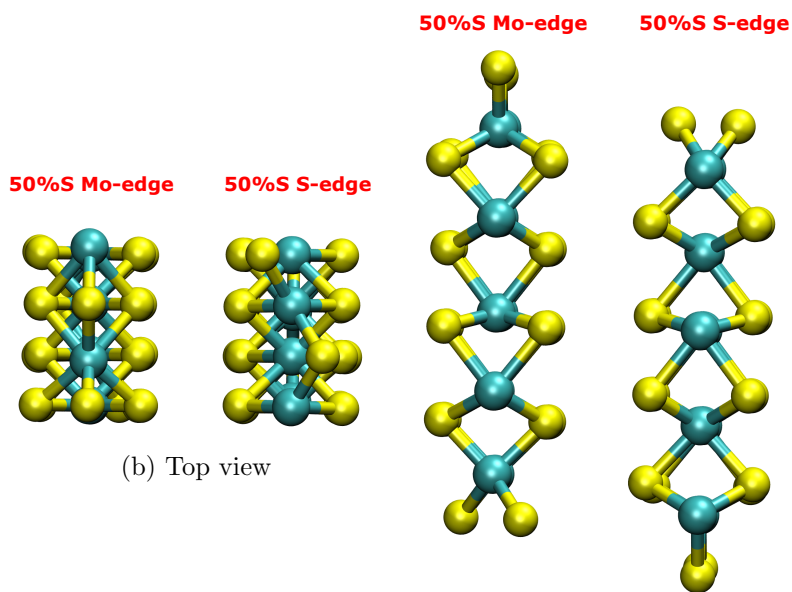
In recent years, transition metal disulfides (TMDs) have attracted much attention due to their abundance, low cost, and catalytic activity.<sup>1-5</sup> Similar to graphite, many TMDs occur in nature as bulk materials consisting of stacked layers. Because of its natural occurrence, and

potential use in numerous applications (from catalysis to solid lubricants),<sup>6</sup> the most studied material in the TMD series is molybdenum disulfide, MoS<sub>2</sub>.<sup>7</sup> Bulk MoS<sub>2</sub> is a non-magnetic indirect semiconductor.<sup>8</sup> However, since it is a 2D material, MoS<sub>2</sub> particles have a basal plane and edges with contrasting chemical properties. There is a general consensus that the edges of the most common 2H-MoS<sub>2</sub> polymorph are the catalytically active sites, while the defect-free basal plane is inert.<sup>9</sup> Even more generally, the chemical, magnetic and electronic properties of the edges tend to dominate the overall performance of the material.<sup>10,11</sup> There are different types of edges in MoS<sub>2</sub> with various properties.<sup>12-14</sup> As represented in Figure 1, two families of edges can be distinguished for 2H-MoS<sub>2</sub>: the armchair edge ( $\bar{1}2\bar{1}0$ ) and the zigzag edges, for which the Mo-edge ( $\bar{1}010$ ) and S-edge ( $10\bar{1}0$ ) have distinct chemical properties.<sup>15</sup> Theoretical<sup>16</sup> and experimental studies,<sup>17,18</sup> show that zigzag edges are much more stable than armchairs, so that experimentally the zigzag edges have been reported as the dominating edge of MoS<sub>2</sub> particles.

Many studies have approached the problem of the edge configuration and their relative stability. Most of these studies have been carried out in the context of the hydrodesulfurization (HDS) reaction, for which MoS<sub>2</sub> is a typical catalyst.<sup>19,20</sup> HDS removes sulfur from natural gas and from petroleum. Therefore, it reduces polluting sulphur dioxide (SO<sub>2</sub>) emissions upon fuel and gas combustion. Under HDS conditions MoS<sub>2</sub> is exposed to a mixture of H<sub>2</sub> and H<sub>2</sub>S gases. Therefore, the relative stability of edges with different sulfidation levels is governed by the relative abundance of H<sub>2</sub> and H<sub>2</sub>S, the first decreasing the S coverage of the edges, the latter increasing it. The first such ab initio thermodynamic model was developed by Raybaud et al.<sup>21</sup> for the zigzag edge based on density functional theory (DFT) computations. This theoretical study suggested that the 100%S S-edge and the 50%S Mo-edge are the most stable sulfidation levels under typical HDS conditions. The 50%S Mo-edge is particularly stable due to the reconstruction of the structure that satisfies the coordination needs of Mo and S atoms. Hence, transformation to more or less sulfided Mo-edges is suggested to be an activated process.<sup>22</sup> For the stoichiometric case, i.e., absence of excess S, the



(a) Different types of MoS<sub>2</sub> edges



(b) Top view

(c) Side view

Figure 1: (a) Classification of MoS<sub>2</sub> edges according to the way a single layer of 1H-MoS<sub>2</sub> is truncated. The crystallographic indices and common names of these edges are given. Two types of edges are shown: Zigzag and armchair edges. Because of the symmetry of MoS<sub>2</sub>, there are two types of zigzag edges: Mo-edge and S-edge, (b) Top and (c) Side views of 50%S S-edge and 50%S Mo-edge. The color code for atoms is yellow for S and greenish for Mo.



most stable distribution of S over the Mo and S edge was predicted to be semi-saturated (50%S) on both edges. This also corresponds to typical sulfur poor conditions.<sup>21,23</sup> Revisiting these conclusions based on more reliable dispersion corrected DFT computations left the main conclusions unchanged.<sup>24</sup> Nevertheless, the prevalent structure of the active sites during hydrodesulfurization catalysis on MoS<sub>2</sub> is still debated.<sup>25</sup>

Complementary to the computational work, various experimental studies have been carried out to determine the structure and stability of MoS<sub>2</sub> edges. For most of these experiments, MoS<sub>2</sub> nanoparticles with different edge types and shapes were synthesised in a controlled atmosphere (generally H<sub>2</sub> and H<sub>2</sub>S) and characterised by scanning tunneling microscopy (STM)<sup>12,13,22,26-32</sup> or transmission electron microscopy (TEM).<sup>33,34</sup> As predicted by experiment, the sulfidation level of the edges was found to vary depending on the equilibrium between hydrogen and sulfur-containing species in the gas-phase.<sup>8,35</sup> Lauritsen et al.<sup>36</sup> synthesized MoS<sub>2</sub> nanoflakes on a gold substrate using sulfur rich and sulfur poor conditions. The STM analysis of the corresponding nanoflakes revealed a predominance of triangular flakes with 100%S Mo-edge and hexagonal flakes with a mixture of 50%S Mo-edge and hydrogenated 100%S S-edge, respectively. Furthermore, the transition between the hexagonal and triangular flakes was found to be an activated process, in agreement with the theoretical studies mentioned above.

In 2005, Hinnemann et al.<sup>37</sup> demonstrated for the first time the potential of MoS<sub>2</sub> as a promising low-cost electrocatalyst for HER through computational and experimental methods. Inspired by this early work,<sup>37</sup> several groups have explored the electrocatalytic activity of molybdenum disulfide and how to improve it.<sup>38,39</sup> Jaramillo et al.<sup>10</sup> synthesized MoS<sub>2</sub> on Au(111) substrate and showed that the electrocatalytic activity of MoS<sub>2</sub> versus HER increases linearly with the total length of the exposed edges of MoS<sub>2</sub>. Tan et al.<sup>40</sup> also presented that the edge site showed much higher activity for HER than the basal plane. Since then, numerous experimental studies have reported that although the edge occupies a small portion of the surface area of MoS<sub>2</sub>, the HER active site is mainly located at the zigzag edges

and only a minority of active sites are located on the basal plane.<sup>1,41-44</sup>

For theoretical identification of active sites, the adsorption energy of hydrogen,  $\Delta G_H$ , is typically used as a descriptor.<sup>45,46</sup> A positive  $\Delta G_H$  value indicates that the interaction between H and MoS<sub>2</sub> is too weak to catalyse the proton electron transfer process. A negative value indicates that the interaction is too strong, i.e., desorbing gaseous H<sub>2</sub> is energetically too costly. The adsorption of hydrogen on the edge of 2H-MoS<sub>2</sub> largely depends on the edge type and the sulfidation level.<sup>34,41,42,47</sup> The most favorable hydrogen bonding with respect to HER was found for the edge covered by sulfur monomers (50%S Mo-edge). This edge is stable under a wide range of sulfidation conditions and should therefore be abundant in the catalytic particles. For all hydrogen coverages between  $\theta_H = 0\%$  and  $\theta_H = 100\%$ , the adsorption energy of hydrogen at 50%S Mo-edge is about 0 eV.<sup>48</sup>

Goddard et al.<sup>49</sup> performed a study of the HER mechanism at the 50%S Mo-edge of the 2H phase MoS<sub>2</sub> based on calculations including Poisson-Boltzmann solvation.<sup>50</sup> They found that HER occurs through the Volmer-Heyrovsky pathway involving electron-rich molybdenum hydride and a hydronium cation. They estimated an energy barrier of 0.19 eV, which agrees very well with the experimental value of 0.21 eV estimated from the turnover frequency (TOF). Their study highlighted the importance of activation energies to identify the actual reaction mechanism, i.e., going beyond purely thermodynamic descriptors. Later work clarified also the role of Mo and S adsorption sites for the HER reaction mechanism, with diffusion steps between the two playing an important role due to kinetic limitations.<sup>51</sup> Furthermore, H<sub>2</sub> desorption was identified as one of the most activated steps.<sup>51</sup>

Although the interaction between hydrogen atoms and the edge of MoS<sub>2</sub> has been extensively studied in the past, there are only few studies on the interaction between water and the edge of MoS<sub>2</sub>, all of them being based on DFT computations, i.e., without experimental validation. Singh et al.,<sup>52</sup> studied water dissociation, including the corresponding activation energies, over the three thermodynamically stable edges reported by Raybaud et al. (0%S Mo-edge, 50%S S-edge, and 100%S S-edge).<sup>21</sup> For 100%S S-edge, the reaction was

found to be endothermic. However, the process is exothermic for both 50%S S-edge and 0%S Mo-edge, with the 0%S Mo-edge having the lowest activation energy barrier. Ab initio molecular dynamics (AIMD) further confirmed a spontaneous dissociation of water on the 0%S Mo-edge, demonstrating that this surface termination is unstable and thus irrelevant in aqueous solution.

The impact of the reactivity of the edges towards water has been investigated as part of our previous study<sup>53</sup> that focused on HER over MoS<sub>2</sub> explicitly accounting for the electrochemical potential via grand-canonical DFT in combination with the linearized Poisson-Boltzmann equation.<sup>54,55</sup> The thermodynamics of proton reduction as a function of electrochemical potential shows that four edge sites of the 0%S Mo-edge and the 100%S S-edge exhibit thermodynamic overpotentials below 0.2 V.<sup>53</sup> Contrary to current proposals, many of these active sites involve adsorbed OH. Hence, we have shown that although H<sub>2</sub>O and OH block "active" sites, HER can also occur on these "blocked" sites, reducing protons on surface OH /H<sub>2</sub>O entities.

Here, we investigate the stability of the MoS<sub>2</sub> edges and the impact on HER of the changes due to reactions with water. While under HDS conditions there is a constant source of sulfur and thus the sulfided edges can be stable, under HER conditions only the chemical potential of hydrogen is well defined. Hence, loss of sulfur atoms in form of H<sub>2</sub>S under these reducing conditions is irreversible. The 50%S Mo-edge and the 50%S S-edge configurations are the most representative ones obtained by the large-scale preparation of MoS<sub>2</sub> catalysts via wet-impregnation followed by sulfidation. The adsorption of H, H<sub>2</sub>O and electrochemically generated OH\* is studied in detail on these edges. Then, we assess the possibility for H<sub>2</sub>S release from these edges. Finally, relying on grand-canonical DFT we demonstrate the possibility of HER even on the desulfided edges via OH/H<sub>2</sub>O cycles.

# Methods

## Computational details

The first-principles calculations are performed using the periodic DFT code "Vienna ab initio simulation package", VASP.<sup>56</sup> We have adopted the generalized gradient approximation density functional PBE-dDsC,<sup>57,58</sup> which is augmented with a density-dependent dispersion correction.<sup>59</sup> The nuclei and core electrons are described by the projector augmented wave function approach (PAW).<sup>60,61</sup> A plane-wave basis set with a kinetic energy cutoff of 500 eV is used for the valence electrons. The precision setting of VASP is set to "accurate". We used a Fermi smearing corresponding to room temperature (0.025 eV) and a Monkhorst-Pack  $3 \times 3 \times 1$  k-point mesh for all the studied surfaces p(2  $\times$  1), p(3  $\times$  1) and p(4  $\times$  1). The convergence criterion for the self-consistency process is set to  $10^{-5}$  eV for the optimization of the wave function. The maximum forces are converged to below 0.025 eV/Å during the geometry optimization. All edges are five layers thick, leading to well converged adsorption energies. Above and below the slabs, approximately 15 Å of vacuum is added in the z-direction.<sup>62</sup> The electrochemical interface is described by the solution of the linearized Poisson-Boltzmann equation as implemented in VASPsol.<sup>54</sup> As in our previous study,<sup>53</sup> the "critical" density,  $\rho_c$  is set to  $0.00025 e^-/\text{Å}^{-3}$ , which is equivalent to one-tenth of the default value in order to prohibit the implicit solvent from entering between the MoS<sub>2</sub> layers. This makes the DFT computations slower than usual due to the associated larger numerical noise, but has also been used previously in the context of solvated alkali-metal ions<sup>63,64</sup> The Debye screening length is set to 3 Å, which corresponds to a 1 M electrolyte. To properly define the work-function (electrochemical potential) of the interface, the dipole moment of the slab needs to be nullified through symmetry. We perform a point symmetrization for all the edges. The central layers are kept frozen in their bulk positions.

## Reaction energies

For isolated molecules we use the following approximation for their free energy:

$$G_{mol} = E_{mol} - TS \quad (1)$$

where  $T$  is room temperature (298.15 K), and  $S$  is the contribution of rotational translational entropy at standard pressure. For water, this entropy contribution is divided by two to account for its liquid state.<sup>65,66</sup>

If not stated otherwise, the adsorption energy,  $\Delta G_{ads}$ , of the different species are calculated in the framework of the computational hydrogen electrode (CHE)<sup>67</sup> at 0 V:

$$G_{ads} = \frac{1}{2} \times (E_{tot} - E_{slab} - R) \quad (2)$$

Where  $E_{tot}$  and  $E_{slab}$  are the energies of the symmetric MoS<sub>2</sub> surface with and without adsorbates, respectively. When the adsorbate is hydrogen (i.e., one hydrogen atom per surface), the energy of the reactant is defined as  $R = G_{H_2(g)}$ , where  $G_{H_2(g)}$  is the free energy of the hydrogen molecule. For the adsorption of the water molecule,  $R = 2G_{H_2O}$ . For OH adsorption under the relevant reducing conditions, we set  $R = G_{H_2(g)} - 2G_{H_2O}$ . In other words, OH\* is formed by adsorption of H<sub>2</sub>O with a subsequent electroreduction (formally a Heyrovsky step) that releases H<sub>2</sub>.<sup>53</sup>

Similarly, we assess the stability of the edges with respect to the release of H<sub>2</sub>S:

$$\Delta G_{release_1} = \frac{1}{2} \times (E_{decomp} + 2G_{H_2S} - E_{tot}) \quad (3)$$

Where  $E_{tot}$  and  $E_{decomp}$  are the energies of the symmetric MoS<sub>2</sub> surface with H<sub>2</sub>S (in the form of at least 50% H coverage on the 50%S edges) and the "decomposed" edge, i.e., after loss of H<sub>2</sub>S, respectively.  $G_{H_2S}$  is the free energy of the H<sub>2</sub>S molecule. If  $G_{release_1}$  is equal to 0 eV, it is an isothermal process. A negative value indicates that the reaction is spontaneous.

A positive value indicates that the process is not spontaneous under standard conditions. Note, however, that under HER conditions the partial pressure of  $\text{H}_2\text{S}$  is essentially zero, so that even endergonic reactions have a finite probability to occur.

An alternative of this "decomposition" reaction is the "substitution" reaction:  $\text{H}_2\text{S}$  can be released in combination with water adsorption. The formula of the release energy is:

$$\Delta G_{\text{release}_2} = \frac{1}{2} \times (E_{\text{subst}} + 2G_{\text{H}_2\text{S}} - E_{\text{tot}} - 2G_{\text{H}_2\text{O}}) \quad (4)$$

Where  $E_{\text{tot}}$  and  $E_{\text{subst}}$  are the energies of the (initial) symmetric  $\text{MoS}_2$  surface with hydrogen bonding to sulfur and the (substituted) edges with hydrogen bonded to oxygen, respectively.  $G_{\text{H}_2\text{S}}$  and  $G_{\text{H}_2\text{O}}$  are the free energies of the  $\text{H}_2\text{S}$  and  $\text{H}_2\text{O}$  molecules. The criterion for determining the thermodynamic nature of the process is the same as for Eq.3.

## Hydrogen production by $\text{H}_2\text{O}$ , OH and O cycling

Our earlier study showed that adsorbed  $\text{OH}^*$  and  $\text{H}_2\text{O}$  species can participate in HER. This  $\text{OH}^*$  differs from the adsorption of  $\text{OH}^-$ , as it is associated with water reduction and should be considered as an adsorbed hydroxyl "radical" and thus accessible in acidic, reducing conditions. Similarly, we here investigate the stability and activity of such active sites on the 50%S S-edge; 50%S Mo-edge. The corresponding catalytic cycle is schematically depicted on Figure 2. Adsorbate  $A_1$ , which is also a reaction intermediate, can be O or OH, while the corresponding intermediate  $A_2$  is OH or  $\text{H}_2\text{O}$ , respectively. In these catalytic cycles, the reactions connecting the intermediates are the addition of a  $\text{H}^+ + \text{e}^-$  pair, with  $\Delta G_1$  resembling a Volmer and  $\Delta G_2$  a Heyrovsky step, respectively. For these catalytic cycles, we perform grand-canonical DFT computations in order to explicitly study the potential dependence. In practice, the charge of the system is varied from  $-1$  to  $+1$  with a step length of  $0.2 e^-$  and it is neutralized via the Poisson-Boltzmann equation in close analogy with our previous works.<sup>53,68</sup> The acquired connection between the grand-canonical energy and

the electrochemical potential is then fitted to an analytical formula, which is a parabola for conductors.

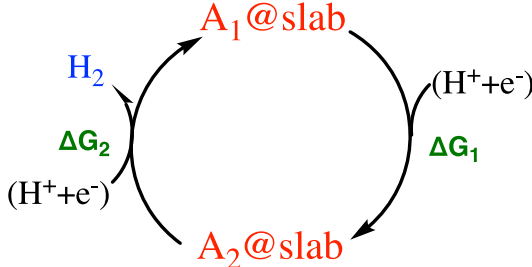


Figure 2: H<sub>2</sub> evolution via cycling between OH and H<sub>2</sub>O or O and OH.  $\Delta G_1$  corresponds to a Volmer step (adsorption of  $H^+ + e^-$ ), while  $\Delta G_2$  is a Heyrovsky step.

Hydrogen production by these cycles can only occur when the  $\Delta G$ s are less than or near zero. They are calculated as a function of the electrochemical potential according to the following formulas:

$$\Delta G_1(U) = \frac{1}{2} \times (E_{tot}(A_2)(U) - E_{tot}(A_1)(U) - 2 \times (H^+ + e^-)) \quad (5)$$

$$\Delta G_2(U) = \frac{1}{2} \times (E_{tot}(A_1)(U) + 2 \times G_{H_2} - E_{tot}(A_2)(U) - 2 \times (H^+ + e^-)) \quad (6)$$

Where  $E_{tot}(A_1)(U)$  and  $E_{tot}(A_2)(U)$  are the potential dependent energies of the symmetric MoS<sub>2</sub> edges with O or OH for  $A_1$  and with OH or H<sub>2</sub>O for  $A_2$ .  $G_{H_2}$  is the free energy of the hydrogen molecule, and  $U$  is the applied potential with respect to the standard hydrogen electrode.

As pointed out by Norskov and coworkers, the chemical potential of protons and electrons can be conveniently replaced by that of hydrogen molecules and the energy correction for the electron due to the electrode potential.<sup>67</sup> Therefore,  $2 \times (H^+ + e^-) = 2\mu_H(U) = G_{H_2(g)} - 2eU$  at pH=0, as we evaluate here HER under acidic conditions.

# Results and discussions

## Hydrogen adsorption

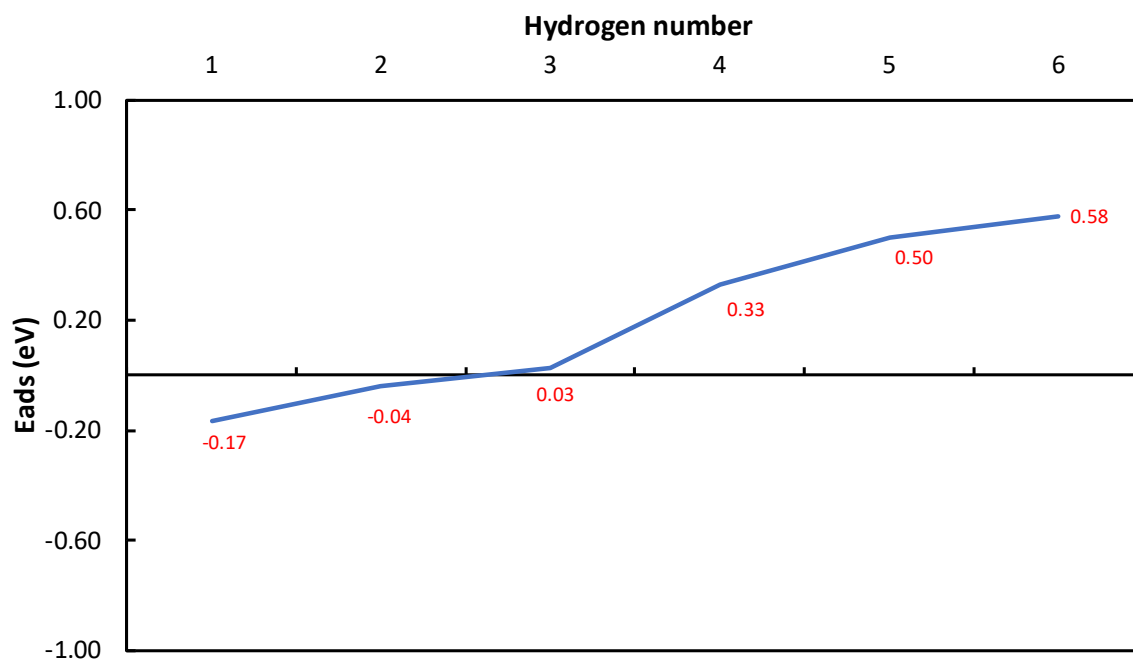
Based on the most stable stoichiometric edge of MoS<sub>2</sub> (reconstructed 50%S S-edge in combination with 50%S Mo-edge, see Figure S1 and Figure 3), we investigated the expected hydrogen coverage in HER conditions. The first step was to locate promising hydrogen adsorption sites (see Figure S2).  $\Delta G_H$  is very close to 0 eV in all cases. The most stable adsorption site is on the "side" of the 50%S S-edge, with an adsorption energies of 0.04 eV. For the second hydrogen adsorption, the most promising sites are the "side" site (-0.01 eV). The top S site is somewhat peculiar: the first hydrogen adsorption energy is endergonic (0.38 eV), while the second one is exergonic (-0.14 eV). Given that the average remains less favorable than the "side" adsorption mode, these top-modes are likely to be relevant only at high H coverages. Based on these results, we investigated the overall hydrogen adsorption as a function of the H coverage for the MoS<sub>2</sub> 50 %S edges. Assessing various combinations, we identified the most stable step-wise H adsorption sequence: hydrogen 1 to 6 as shown in Figure 3. With increasing  $\theta_H$ , the  $\Delta G_H$  becomes weaker which is in complete agreement with the previously reported results of MoS<sub>2</sub><sup>69</sup> and with other transition metal dichalcogenides and phosphides in general.<sup>70,71</sup>  $\Delta G_H$  of the first to the fourth hydrogen is very close to 0 eV (from -0.17 eV to 0.33 eV). This opens the possibility for H<sub>2</sub> release via the Volmer-Tafel mechanism under the condition that the activation energy for the (chemical) Tafel step is not too high.

## H<sub>2</sub>O/OH adsorption and H co-adsorption

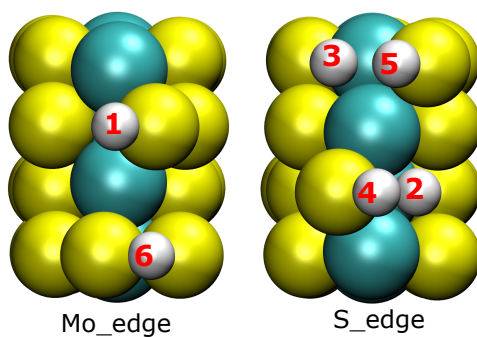
We now move to the adsorption of the solvent (H<sub>2</sub>O) and OH which can be generated under HER conditions on the MoS<sub>2</sub> edges.<sup>53</sup>

As illustrated in Figure 4, H<sub>2</sub>O adsorption is nearly thermoneutral for both the 50%S S-edge and the 50%S Mo-edge. For the 50%S S-edge, where H<sub>2</sub>O is more strongly adsorbed,



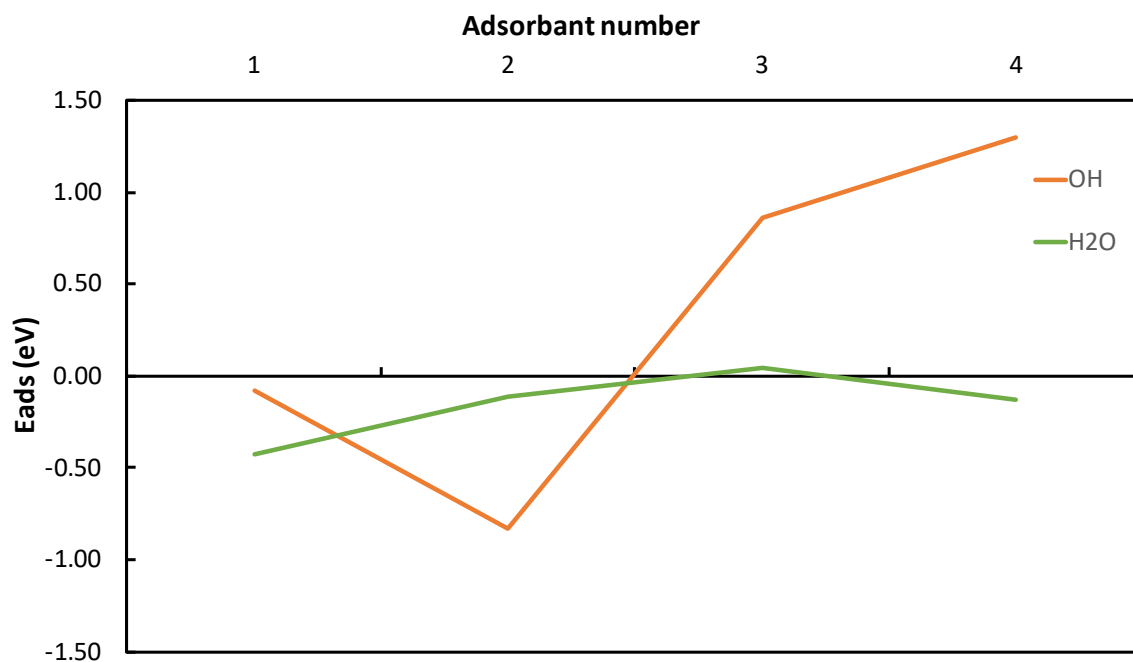


(a) The Hydrogen adsorption energies as a function of the Hydrogen coverage.



(b) Visualization of the MoS<sub>2</sub> edges with the different hydrogen adsorbed.

Figure 3: Hydrogen adsorption on 50%S S-edge and 50%S Mo-edge .The color code for atoms is white for H; yellow for S and greenish for Mo.



(a) adsorption energies of OH and H<sub>2</sub>O on the different edge sites.

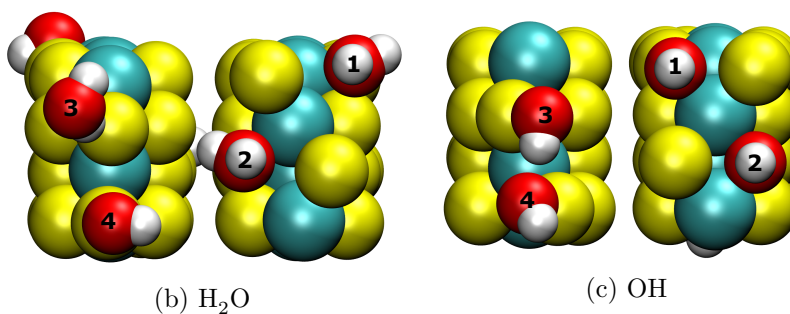


Figure 4: The adsorption energies of OH and H<sub>2</sub>O on MoS<sub>2</sub> edges with visualisation of the structures. The color code for atoms is white for H; red for O; yellow for S and greenish for Mo.

the oxygen atom is in the "side" position and one hydrogen atom points away from the surface, while the other lies in the surface plane, pointing toward the neighboring MoS<sub>2</sub> layer. At the 50%S Mo-edge, the water molecules are just physisorbed, with one hydrogen atom pointing towards the sulfur surface atom, establishing the closest contact between water and the surface. For both edges, the OH bond lengths in the adsorbed water molecule are slightly larger (0.978 Å) than those of a free H<sub>2</sub>O molecule (0.958 Å), indicating that the OH bond is slightly weakened when the molecule is in contact with the MoS<sub>2</sub> edge.

In contrast to H<sub>2</sub>O, OH is only adsorbed at the 50%S S-edge, especially when there is one  $\theta_{OH} = 1$ . The OH adsorption energy on the 50%S Mo-edge is, however, above 1 eV. This difference is explained by the accessibility of the Mo atom in the "side" adsorption mode on the 50%S S-edge, while the Mo atoms of the 50%S Mo-edge are completely inaccessible.

These results reveal that there is a competition between H and OH at the 50%S S-edge, while H<sub>2</sub>O seems to be rather labile over both edges.

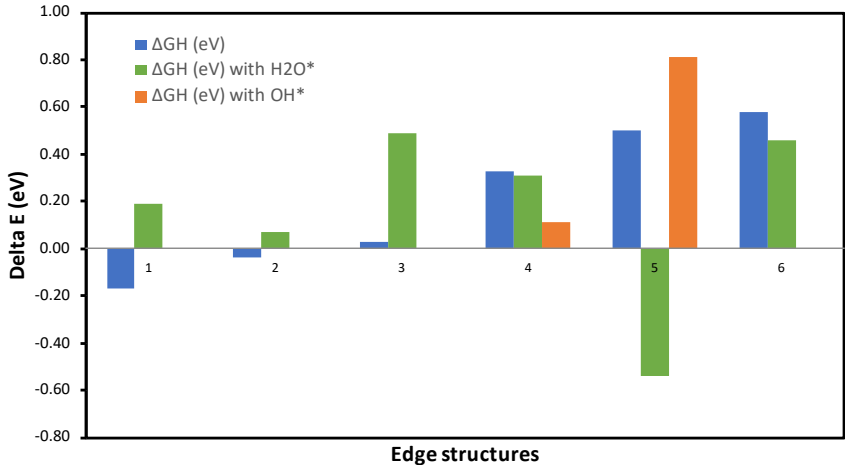


Figure 5: Comparison of the different  $\Delta G_H$  values without and with the presence of OH and H<sub>2</sub>O. The numbering of the H atoms is the same as in Fig. 3

In view of the competition of H and OH and knowing that H<sub>2</sub>O will be present anyway, we assess  $\Delta G_H$  in the presence of OH and H<sub>2</sub>O. The different combinations tested are reported on Figure S3, while Figure 5 summarizes  $\Delta G_H$  for the various cases. Note that our tests show that the adsorption energy of one species is not affected by the presence of another

molecule at the "other" edge, i.e., the Mo-edge and S-edge can be considered "decoupled" (see Figure S4).

For the 50%S Mo-edge, we observe that the presence of H<sub>2</sub>O does not qualitatively change the conclusion: The first hydrogen atom (number 1 in Fig. 5 is weakly adsorbed (the sign changes in presence/absence of water, but the adsorption energy remains weak), while the second one (number 6) features a clearly positive adsorption energy. For the 50%S S-edge, hydrogen number 2 and 4 are not affected by H<sub>2</sub>O, i.e., green and blue bars are close to each other. This is not the case for hydrogen 3, for which  $\Delta G_H$  reaches 0.49 eV in presence of H<sub>2</sub>O, while it was thermoneutral in the absence of the water molecule. Hydrogen 5 "compensates" this endothermicity, i.e. it is very strongly adsorbed in the presence of water, while it was costly in the absence of co-adsorption (-0.54 eV and 0.5 eV, respectively). The case of OH co-adsorption is restricted to hydrogen 4 and 5: The OH take the place of hydrogen 2 and 3. The effect of OH on hydrogen 4 is only  $\sim 0.2$  eV, making H adsorption nearly thermoneutral. However, adsorbing a second hydrogen atom (number 5) becomes prohibitive  $\Delta G_H = 0.8$  eV.

In summary, water modulates the hydrogen adsorption energy, but, in agreement with the weak adsorption energy of water on these edges, the overall H coverage is only marginally affected by the solvent. In contrast, the presence of OH groups on the "side" positions of the 50%S S-edge, where they are easily formed (see Fig. 4), reduces the H coverage on the S-edge significantly.

## Edge Stability

An important aspect of MoS<sub>2</sub> electrocatalysts is their (long-term) stability. In contrast to HDS applications, there is no sulfur reservoir under HER conditions. Hence, we here estimate the thermodynamic stability of the edges. As shown in two preceding sections, the hydrogen coverage is significant ( $\sim 1$  monolayer (ML) with respect to the Mo edge atoms) under HER conditions. Therefore, we start by computing the reaction energy for H<sub>2</sub>S release (see Figure

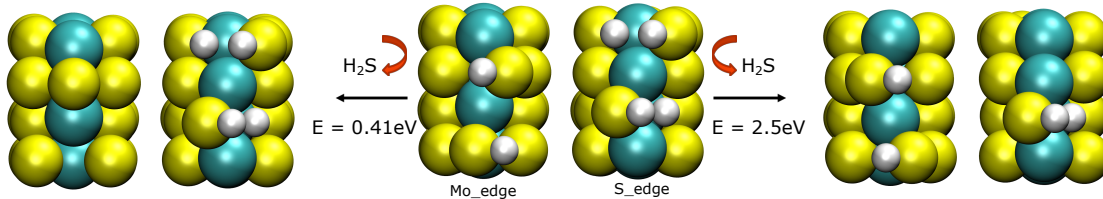


Figure 6:  $\text{H}_2\text{S}$  release on 50% S Mo-edge and 50% S S-edge after H adsorption. The color code for atoms is white for H; yellow for S and greenish for Mo.

6), a typical process known in the literature in the context of hydrogen rich HDS conditions. At the 50%S S-edge, we find that the process is very endothermic (2.5 eV). In contrast, the 50%S Mo-edge is significantly less stable and  $\text{H}_2\text{S}$  desorption is endergonic by only 0.41 eV. Note that this reaction energy assumes standard conditions (1 bar of  $\text{H}_2\text{S}$ ). Hence, under HER conditions (no partial pressure of  $\text{H}_2\text{S}$ ), the loss of  $\text{H}_2\text{S}$  is certainly facilitated compared to this estimate. Furthermore, in the absence of a S reservoir, any sulfur that is lost from the surface has no chance to be replenished. Hence, we conclude that the sulfur coverage of the 50%S Mo-edge will decrease over time until it reaches the 0%S Mo-edge. Fortunately for HER, this edge is expected to be reasonably active as well,<sup>53</sup> so that activity should not drop significantly over time despite the structural rearrangements. As for the 50%S S-edge, it seems to be stable in the presence of H, i.e., the adsorbed hydrogen atoms can participate in the HER mechanism.

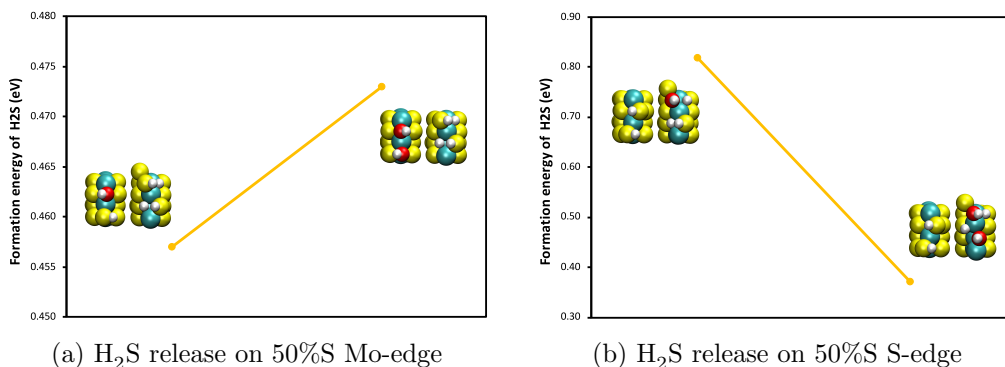


Figure 7:  $\text{H}_2\text{S}$  release on 50%S Mo-edge and 50%S S-edge after OH adsorption. The color code for atoms is white for H; red for O; yellow for S and greenish for Mo.

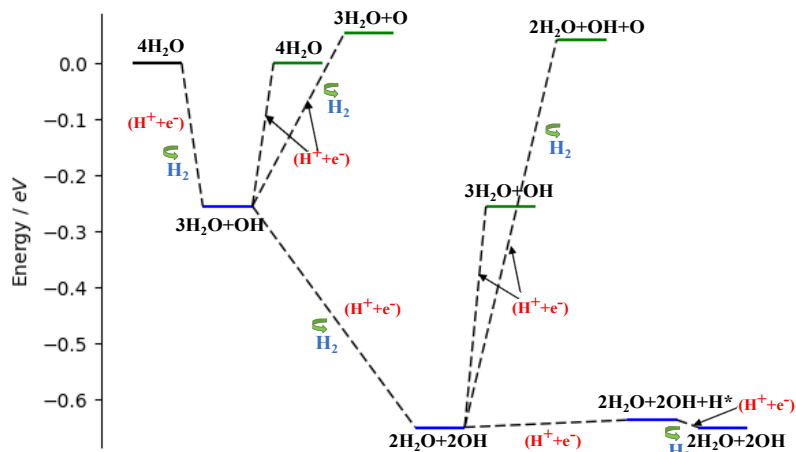
The above estimates have been performed without the consideration of the actual reaction

medium which is an aqueous solution. As discussed above, OH can be generated in situ under HER conditions. Hence, we here investigate an "exchange" reaction, where the edge sulfur atoms are replaced by oxygen. To be precise, we assess the following reaction:  $E-SH + H_2O \longrightarrow E-OH + H_2S$ , where "E" symbolizes the remaining atoms of the edge. Figure 7 shows that for the Mo-edge it is possible to release  $H_2S$  with nearly the same exchange reaction energy for the first OH as for the second OH (0.4-0.5 eV). Furthermore, this energy is very similar to the loss of  $H_2S$  of Fig. 6. For the S-edge, the exchange reaction energy is significantly more energy consuming for the first OH (0.8 eV) than for the Mo-edge, although still much lower than the  $H_2S$  desorption energy. However, replacing the second OH by SH is as feasible as on the Mo edge.

These results indicate that the stability of the 50%S Mo-edge is rather limited under HER condition, which  $H_2S$  desorption, potentially assisted by  $H_2O/OH$  adsorption being rather likely. The 50% S-edge is somewhat more stable. Nevertheless, in the absence of estimates concerning the reaction barrier for the  $E-SH \longrightarrow E-OH$  exchange reaction under HER conditions, it is difficult to judge how much this decomposition reaction contributes to the long-term (in-)stability of the  $MoS_2$  electrocatalyst. It must be noted that the 0%S Mo-edge is likely to remain active for HER.<sup>53</sup> This is, however, not the case for the 0%S S-edge: According to our computations (see Fig. S5), this edge termination is permanently blocked by OH, rendering this edge inactive for HER.

## **HER mechanism over 50%S S-edge in presence of water**

As shown above, the  $MoS_2$  edges react with the water solvent under HER conditions. Hence, we here revisit the HER reaction mechanism starting with the most relevant surface state. In particular, the 50%S S-edge is likely to be partially covered by OH. For the Mo-edge, the adsorbed water molecules are very unlikely to dissociate, since OH is poorly adsorbed (see OH 3 and 4 of Fig. 4). To assess the possibility of hydrogen production, we assessed different catalytic cycles. For the S-edge, Figure 8 shows the most relevant energy profile at 0 V. We



(a) Reaction energy profile at 0 V

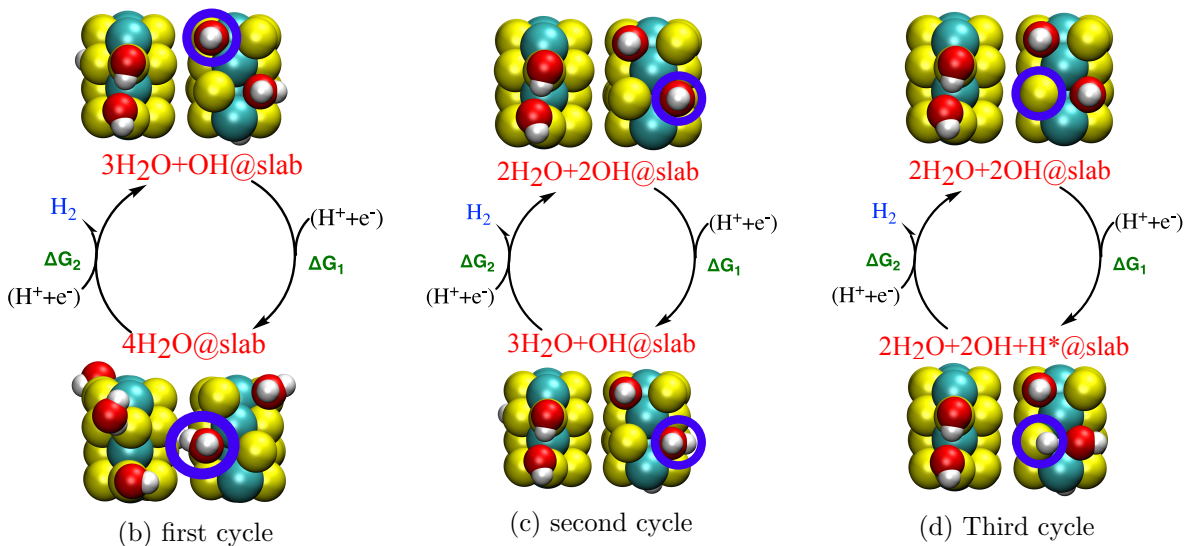


Figure 8: (a) Production of  $\text{H}_2$  on the water covered S-edge, involving  $\text{H}_2\text{O}$ , OH and  $\text{H}^*$ . The thermodynamic over-potential  $\eta_{TD}$  is determined to be 0 V. The possible steps are designed by the blue color whereas the green color is for the blocking steps. (b) The first cycle with  $\Delta G_1 = 0.225$  eV and  $\Delta G_2 = -0.225$  eV. (c) The second cycle with  $\Delta G_1 = 0.394$  eV and  $\Delta G_2 = -0.394$  eV. (d) The third cycle with  $\Delta G_1 = 0.014$  eV and  $\Delta G_2 = -0.014$  eV. The color code for atoms is white for H; red for O; yellow for S and greenish for Mo. The circle blue indicates the site where the different steps occur.

start with the edge structure on which four water molecules are physisorbed, two spectators at the Mo-edge and the other two at the S-edge. At this potential, the Heyrovsky reaction releasing  $\text{H}_2$  and concomitantly forming OH on the S-edge is exothermic. At this stage there are three pathways, two of which are endothermic, so we continue with the exothermic one, which leads to two OH adsorbed on the S edge. This surface state still presents three possible paths that could lead to HER: A Heyrovsky step with an OH hydrogen, a Volmer step on an OH, or a Volmer step on an S site. Our grand-canonical DFT computations demonstrate that only the latter is energetically feasible, leading to S-H. Several reactions could proceed with this S-H (see Fig. S6): (i) in combination with an additional proton reduction  $\text{H}_2\text{S}$  could be released, (ii) an  $\text{SH}^*/\text{OH}^*$  exchange reaction or (iii)  $\text{H}_2$  production via a Heyrovsky step. The first of these reactions one is strongly endothermic. The second one is mildly endothermic (0.2 eV) and thus likely to be feasible but slow under HER conditions. However, once this reaction occurs and we reach an edge covered by 3  $\text{OH}^*$ , on which the Volmer step is endergonic by 0.4 eV, so that the HER activity is lost. The last possibility is the HER reaction, which turns out to be athermic as indicated in Fig. 8d.

Therefore, we demonstrate that despite the presence of two surface OH entities on the 50%S S-edge, the sulfur sites could remain catalytically active via a Volmer Heyrovsky mechanism at near zero overpotential.

## Conclusion

We have analyzed the fate of the most commonly produced  $\text{MoS}_2$  edge, i.e., the 50%S S-edge; 50%S Mo-edge, under HER conditions. While this Mo-edge could potentially be active for HER with an estimated overpotential of about 0.2 V, we reveal that this edge is very likely to significantly reconstruct in the presence of water. In particular,  $\text{H}_2\text{S}$  formation is only mildly endothermic ( $\sim 0.4$  eV), so that under HER conditions, where there is no sulfur reservoir, surface-sulfur is gradually replaced by oxygen. Fortunately, the thus formed



surface OH are active sites for HER. The situation on the 50%S-edge is less straight forward. First, the termination is more stable with respect to H<sub>2</sub>S release ( $\Delta G = 2.5$  eV). Second, though, the exchange reaction that replaces surface SH by surface OH is endothermic by only 0.8 eV. Once the first such exchange reactions has occurred, the second one is facilitated. Furthermore, this OH substituted S-edge is no longer predicted to be active for HER. Hence, this exchange reaction appears to lead to a definite loss of HER activity of MoS<sub>2</sub>. Third, our grand-canonical DFT computations suggest that before the loss of surface sulfur, the S atoms of this edge are active sites for HER even in the presence of surface OH, with an estimated overpotential of 0 V.

In summary, our findings provide an atomistic description of the fate of the common 50%S S-edge, 50%S Mo-edge edge structure of MoS<sub>2</sub> under HER conditions. The likely active sites in presence of water have been identified and their stability has been assessed, revealing long-term stability issues of the S-edge in water, a prediction that could be experimentally verified by operando X-ray spectroscopies.

## Acknowledgement

This work was financially supported by Région Auvergne Rhône-Alpes through the project Pack Ambition Recherche 2018 MoSHi. We are very grateful to IFP Energies nouvelles for supporting the MoSHy project (N° 1801167601) and to the IFP Energies nouvelles team, Mona Marie Obadia and Quentin Cacciuttolo, for fruitful discussions. The authors thank the SYSPROD project and AXELERA Pôle de Compétitivité for financial support (PSMN Data Center).

## Supporting Information Available

The supplementary material contains the discussion of the stability of the 50%S reconstructions of the MoS<sub>2</sub> edge, additional Figures and Tables. Coordinates and DFT raw data is

## References

- (1) Laursen, A. B.; Kegnæs, S.; Dahl, S.; Chorkendorff, I. Molybdenum sulfides—efficient and viable materials for electro- and photoelectrocatalytic hydrogen evolution. *Energy & Environmental Science* **2012**, *5*, 5577–5591.
- (2) Wang, H.; Lu, Z.; Xu, S.; Kong, D.; Cha, J. J.; Zheng, G.; Hsu, P.-C.; Yan, K.; Bradshaw, D.; Prinz, F. B., et al. Electrochemical tuning of vertically aligned MoS<sub>2</sub> nanofilms and its application in improving hydrogen evolution reaction. *Proceedings of the National Academy of Sciences* **2013**, *110*, 19701–19706.
- (3) Voiry, D.; Yamaguchi, H.; Li, J.; Silva, R.; Alves, D. C.; Fujita, T.; Chen, M.; Asefa, T.; Shenoy, V. B.; Eda, G., et al. Enhanced catalytic activity in strained chemically exfoliated WS<sub>2</sub> nanosheets for hydrogen evolution. *Nature materials* **2013**, *12*, 850–855.
- (4) Tan, C.; Zhang, H. Two-dimensional transition metal dichalcogenide nanosheet-based composites. *Chemical Society Reviews* **2015**, *44*, 2713–2731.
- (5) Karunadasa, H. I.; Montalvo, E.; Sun, Y.; Majda, M.; Long, J. R.; Chang, C. J. A molecular MoS<sub>2</sub> edge site mimic for catalytic hydrogen generation. *Science* **2012**, *335*, 698–702.
- (6) Chhowalla, M.; Shin, H. S.; Eda, G.; Li, L.-J.; Loh, K. P.; Zhang, H. The chemistry of two-dimensional layered transition metal dichalcogenide nanosheets. *Nature chemistry* **2013**, *5*, 263–275.
- (7) Song, I.; Park, C.; Choi, H. C. Synthesis and properties of molybdenum disulphide: from bulk to atomic layers. *Rsc Advances* **2015**, *5*, 7495–7514.

- (8) Ganatra, R.; Zhang, Q. Few-layer MoS<sub>2</sub>: a promising layered semiconductor. *ACS nano* **2014**, *8*, 4074–4099.
- (9) Lei, B.; Li, G.; Gao, X. Morphology dependence of molybdenum disulfide transparent counter electrode in dye-sensitized solar cells. *Journal of Materials Chemistry A* **2014**, *2*, 3919–3925.
- (10) Jaramillo, T. F.; Jørgensen, K. P.; Bonde, J.; Nielsen, J. H.; Horch, S.; Chorkendorff, I. Identification of active edge sites for electrochemical H<sub>2</sub> evolution from MoS<sub>2</sub> nanocatalysts. *science* **2007**, *317*, 100–102.
- (11) Wang, H.; Zhang, Q.; Yao, H.; Liang, Z.; Lee, H.-W.; Hsu, P.-C.; Zheng, G.; Cui, Y. High electrochemical selectivity of edge versus terrace sites in two-dimensional layered MoS<sub>2</sub> materials. *Nano letters* **2014**, *14*, 7138–7144.
- (12) Schweiger, H.; Raybaud, P.; Kresse, G.; Toulhoat, H. Shape and edge sites modifications of MoS<sub>2</sub> catalytic nanoparticles induced by working conditions: a theoretical study. *Journal of Catalysis* **2002**, *207*, 76–87.
- (13) Füchtbauer, H. G.; Tuxen, A. K.; Li, Z.; Topsøe, H.; Lauritsen, J. V.; Besenbacher, F. Morphology and atomic-scale structure of MoS<sub>2</sub> nanoclusters synthesized with different sulfiding agents. *Topics in Catalysis* **2014**, *57*, 207–214.
- (14) Liu, Y.; Wang, H.; Yuan, X.; Wu, Y.; Wang, H.; Tan, Y. Z.; Chew, J. W. Roles of sulfur-edge sites, metal-edge sites, terrace sites, and defects in metal sulfides for photocatalysis. *Chem Catalysis* **2021**,
- (15) Yu, S.; Zheng, W. Fundamental insights into the electronic structure of zigzag MoS<sub>2</sub> nanoribbons. *Physical Chemistry Chemical Physics* **2016**, *18*, 4675–4683.
- (16) Cao, D.; Shen, T.; Liang, P.; Chen, X.; Shu, H. Role of chemical potential in flake shape

- and edge properties of monolayer MoS<sub>2</sub>. *The Journal of Physical Chemistry C* **2015**, *119*, 4294–4301.
- (17) Wang, Z.; Li, H.; Liu, Z.; Shi, Z.; Lu, J.; Suenaga, K.; Joung, S.-K.; Okazaki, T.; Gu, Z.; Zhou, J., et al. Mixed low-dimensional nanomaterial: 2D ultranarrow MoS<sub>2</sub> inorganic nanoribbons encapsulated in quasi-1D carbon nanotubes. *Journal of the American Chemical Society* **2010**, *132*, 13840–13847.
- (18) Xu, H.; Ding, Z.; Nai, C. T.; Bao, Y.; Cheng, F.; Tan, S. J.; Loh, K. P. Controllable synthesis of 2D and 1D MoS<sub>2</sub> nanostructures on Au surface. *Advanced Functional Materials* **2017**, *27*, 1603887.
- (19) Byskov, L. S.; Nørskov, J. K.; Clausen, B. S.; Topsøe, H. DFT calculations of unpromoted and promoted MoS<sub>2</sub>-based hydrodesulfurization catalysts. *Journal of Catalysis* **1999**, *187*, 109–122.
- (20) Sharifvaghefi, S.; Yang, B.; Zheng, Y. New insights on the role of H<sub>2</sub>S and sulfur vacancies on dibenzothiophene hydrodesulfurization over MoS<sub>2</sub> edges. *Applied Catalysis A: General* **2018**, *566*, 164–173.
- (21) Raybaud, P.; Hafner, J.; Kresse, G.; Kasztelan, S.; Toulhoat, H. Ab initio study of the H<sub>2</sub>-H<sub>2</sub>S/MoS<sub>2</sub> gas–solid interface: The nature of the catalytically active sites. *Journal of Catalysis* **2000**, *189*, 129–146.
- (22) Bollinger, M.; Jacobsen, K. W.; Nørskov, J. K. Atomic and electronic structure of MoS<sub>2</sub> nanoparticles. *Physical Review B* **2003**, *67*, 085410.
- (23) Cristol, S.; Paul, J.; Payen, E.; Bougeard, D.; Clémendot, S.; Hutschka, F. Theoretical study of the MoS<sub>2</sub> (100) surface: a chemical potential analysis of sulfur and hydrogen coverage. *The Journal of Physical Chemistry B* **2000**, *104*, 11220–11229.

- (24) Rosen, A. S.; Notestein, J. M.; Snurr, R. Q. Comprehensive phase diagrams of MoS<sub>2</sub> edge sites using dispersion-corrected DFT free energy calculations. *The Journal of Physical Chemistry C* **2018**, *122*, 15318–15329.
- (25) Mom, R. V.; Louwen, J. N.; Frenken, J. W.; Groot, I. M. In situ observations of an active MoS<sub>2</sub> model hydrodesulfurization catalyst. *Nature communications* **2019**, *10*, 1–8.
- (26) Lauritsen, J.; Nyberg, M.; Nørskov, J. K.; Clausen, B.; Topsøe, H.; Lægsgaard, E.; Besenbacher, F. Hydrodesulfurization reaction pathways on MoS<sub>2</sub> nanoclusters revealed by scanning tunneling microscopy. *Journal of Catalysis* **2004**, *224*, 94–106.
- (27) Lauritsen, J. V.; Kibsgaard, J.; Helveg, S.; Topsøe, H.; Clausen, B. S.; Lægsgaard, E.; Besenbacher, F. Size-dependent structure of MoS<sub>2</sub> nanocrystals. *Nature nanotechnology* **2007**, *2*, 53–58.
- (28) Helveg, S.; Lauritsen, J. V.; Lægsgaard, E.; Stensgaard, I.; Nørskov, J. K.; Clausen, B.; Topsøe, H.; Besenbacher, F. Atomic-scale structure of single-layer MoS<sub>2</sub> nanoclusters. *Physical review letters* **2000**, *84*, 951.
- (29) Bruix, A.; Füchtbauer, H. G.; Tuxen, A. K.; Walton, A. S.; Andersen, M.; Porsgaard, S.; Besenbacher, F.; Hammer, B.; Lauritsen, J. V. In situ detection of active edge sites in single-layer MoS<sub>2</sub> catalysts. *ACS nano* **2015**, *9*, 9322–9330.
- (30) Tuxen, A.; Kibsgaard, J.; Gøbel, H.; Lægsgaard, E.; Topsøe, H.; Lauritsen, J. V.; Besenbacher, F. Size threshold in the dibenzothiophene adsorption on MoS<sub>2</sub> nanoclusters. *Acs Nano* **2010**, *4*, 4677–4682.
- (31) Grønborg, S. S.; Salazar, N.; Bruix, A.; Rodríguez-Fernández, J.; Thomsen, S. D.; Hammer, B.; Lauritsen, J. V. Visualizing hydrogen-induced reshaping and edge activation in MoS<sub>2</sub> and Co-promoted MoS<sub>2</sub> catalyst clusters. *Nature communications* **2018**, *9*, 1–11.

- (32) Kibsgaard, J.; Lauritsen, J. V.; Lægsgaard, E.; Clausen, B. S.; Topsøe, H.; Besenbacher, F. Cluster- support interactions and morphology of MoS<sub>2</sub> nanoclusters in a graphite-supported hydrotreating model catalyst. *Journal of the American Chemical Society* **2006**, *128*, 13950–13958.
- (33) Kisielowski, C.; Ramasse, Q. M.; Hansen, L. P.; Brorson, M.; Carlsson, A.; Molenbroek, A. M.; Topsøe, H.; Helveg, S. Imaging MoS<sub>2</sub> Nanocatalysts with Single-Atom Sensitivity. *Angewandte Chemie International Edition* **2010**, *49*, 2708–2710.
- (34) Hansen, L. P.; Ramasse, Q. M.; Kisielowski, C.; Brorson, M.; Johnson, E.; Topsøe, H.; Helveg, S. Atomic-scale edge structures on industrial-style MoS<sub>2</sub> nanocatalysts. *Angewandte Chemie International Edition* **2011**, *50*, 10153–10156.
- (35) Perticarari, S.; Sayed-Ahmad-Baraza, Y.; Ewels, C.; Moreau, P.; Guyomard, D.; Poizot, P.; Odobel, F.; Gaubicher, J. Dual anion–cation reversible insertion in a bipyridinium–diamide triad as the negative electrode for aqueous batteries. *Advanced Energy Materials* **2018**, *8*, 1701988.
- (36) Lauritsen, J.; Bollinger, M.; Lægsgaard, E.; Jacobsen, K. W.; Nørskov, J. K.; Clausen, B.; Topsøe, H.; Besenbacher, F. Atomic-scale insight into structure and morphology changes of MoS<sub>2</sub> nanoclusters in hydrotreating catalysts. *Journal of Catalysis* **2004**, *221*, 510–522.
- (37) Hinnemann, B.; Moses, P. G.; Bonde, J.; Jørgensen, K. P.; Nielsen, J. H.; Horch, S.; Chorkendorff, I.; Nørskov, J. K. Biomimetic hydrogen evolution: MoS<sub>2</sub> nanoparticles as catalyst for hydrogen evolution. *Journal of the American Chemical Society* **2005**, *127*, 5308–5309.
- (38) Yan, Y.; Xia, B.; Xu, Z.; Wang, X. Recent development of molybdenum sulfides as advanced electrocatalysts for hydrogen evolution reaction. *Acs Catalysis* **2014**, *4*, 1693–1705.

- (39) Pumera, M.; Sofer, Z.; Ambrosi, A. Layered transition metal dichalcogenides for electrochemical energy generation and storage. *Journal of Materials Chemistry A* **2014**, *2*, 8981–8987.
- (40) Tan, S. M.; Ambrosi, A.; Sofer, Z.; Huber, Š.; Sedmidubský, D.; Pumera, M. Pristine basal-and edge-plane-oriented molybdenite MoS<sub>2</sub> exhibiting highly anisotropic properties. *Chemistry–A European Journal* **2015**, *21*, 7170–7178.
- (41) Bonde, J.; Moses, P. G.; Jaramillo, T. F.; Nørskov, J. K.; Chorkendorff, I. Hydrogen evolution on nano-particulate transition metal sulfides. *Faraday discussions* **2009**, *140*, 219–231.
- (42) Tsai, C.; Chan, K.; Abild-Pedersen, F.; Nørskov, J. K. Active edge sites in MoSe<sub>2</sub> and WSe<sub>2</sub> catalysts for the hydrogen evolution reaction: a density functional study. *Physical Chemistry Chemical Physics* **2014**, *16*, 13156–13164.
- (43) Cheng, C.-C.; Lu, A.-Y.; Tseng, C.-C.; Yang, X.; Hedhili, M. N.; Chen, M.-C.; Wei, K.-H.; Li, L.-J. Activating basal-plane catalytic activity of two-dimensional MoS<sub>2</sub> monolayer with remote hydrogen plasma. *Nano Energy* **2016**, *30*, 846–852.
- (44) An, Y.-R.; Fan, X.-L.; Luo, Z.-F.; Lau, W.-M. Nanopolygons of monolayer MS<sub>2</sub>: best morphology and size for HER catalysis. *Nano letters* **2017**, *17*, 368–376.
- (45) Nørskov, J. K.; Bligaard, T.; Logadottir, A.; Kitchin, J. R.; Chen, J. G.; Pandelov, S.; Stimming, U. Trends in the Exchange Current for Hydrogen Evolution. *J. Electrochem. Soc.* **2005**, *152*, J23, Publisher: IOP Publishing.
- (46) Parsons, R. The rate of electrolytic hydrogen evolution and the heat of adsorption of hydrogen. *Trans. Faraday Soc.* **1958**, *54*, 1053–1063, Publisher: The Royal Society of Chemistry.

- (47) Zhou, W.; Zou, X.; Najmaei, S.; Liu, Z.; Shi, Y.; Kong, J.; Lou, J.; Ajayan, P. M.; Yakobson, B. I.; Idrobo, J.-C. Intrinsic structural defects in monolayer molybdenum disulfide. *Nano letters* **2013**, *13*, 2615–2622.
- (48) Kronberg, R.; Hakala, M.; Holmberg, N.; Laasonen, K. Hydrogen adsorption on MoS<sub>2</sub>-surfaces: A DFT study on preferential sites and the effect of sulfur and hydrogen coverage. *Physical Chemistry Chemical Physics* **2017**, *19*, 16231–16241.
- (49) Huang, Y.; Nielsen, R. J.; Goddard III, W. A.; Soriaga, M. P. The reaction mechanism with free energy barriers for electrochemical dihydrogen evolution on MoS<sub>2</sub>. *Journal of the American Chemical Society* **2015**, *137*, 6692–6698.
- (50) Tannor, D. J.; Marten, B.; Murphy, R.; Friesner, R. A.; Sitkoff, D.; Nicholls, A.; Honig, B.; Ringnalda, M.; Goddard III, W. A. Accurate first principles calculation of molecular charge distributions and solvation energies from ab initio quantum mechanics and continuum dielectric theory. *Journal of the American Chemical Society* **1994**, *116*, 11875–11882.
- (51) Li, W.; Liu, G.; Li, J.; Wang, Y.; Ricardez-Sandoval, L.; Zhang, Y.; Zhang, Z. Hydrogen evolution reaction mechanism on 2H-MoS<sub>2</sub> electrocatalyst. *Applied Surface Science* **2019**, *498*, 143869.
- (52) Ghuman, K. K.; Yadav, S.; Singh, C. V. Adsorption and dissociation of H<sub>2</sub>O on monolayered MoS<sub>2</sub> edges: Energetics and mechanism from ab initio simulations. *The Journal of Physical Chemistry C* **2015**, *119*, 6518–6529.
- (53) Abidi, N.; Bonduelle-Skrzypczak, A.; Steinmann, S. N. Revisiting the Active Sites at the MoS<sub>2</sub>/H<sub>2</sub>O Interface via Grand-Canonical DFT: The Role of Water Dissociation. *ACS applied materials & interfaces* **2020**, *12*, 31401–31410.
- (54) Mathew, K.; Kolluru, V. S. C.; Mula, S.; Steinmann, S. N.; Hennig, R. G. Implicit self-



- consistent electrolyte model in plane-wave density-functional theory. *J. Chem. Phys.* **2019**, *151*, 234101.
- (55) Abidi, N.; Lim, K. R. G.; Seh, Z. W.; Steinmann, S. N. Atomistic modeling of electrocatalysis: Are we there yet? *WIREs Computational Molecular Science* n/a, e1499.
- (56) Kresse, G.; Furthmüller, J. Efficiency of ab-initio total energy calculations for metals and semiconductors using a plane-wave basis set. *Computational Materials Science* **1996**, *6*, 15–50.
- (57) Perdew, J. P.; Burke, K.; Ernzerhof, M. Generalized gradient approximation made simple. *Physical review letters* **1996**, *77*, 3865.
- (58) Steinmann, S. N.; Corminboeuf, C. Comprehensive benchmarking of a density-dependent dispersion correction. *Journal of chemical theory and computation* **2011**, *7*, 3567–3577.
- (59) Steinmann, S. N.; Sautet, P.; Michel, C. Solvation free energies for periodic surfaces: comparison of implicit and explicit solvation models. *Physical Chemistry Chemical Physics* **2016**, *18*, 31850–31861.
- (60) Blochl, P. E. Projector augmented-wave method. *Phys. Rev. B* **1994**, *50*, 17953.
- (61) Kresse, G.; Joubert, D. From ultrasoft pseudopotentials to the projector augmented-wave method. *Phys. Rev. B* **1999**, *59*, 1758.
- (62) Steinmann, S. N.; Sautet, P. Assessing a first-principles model of an electrochemical interface by comparison with experiment. *The Journal of Physical Chemistry C* **2016**, *120*, 5619–5623.
- (63) Steinmann, S. N.; Michel, C.; Schwiedernoch, R.; Sautet, P. Impacts of electrode potentials and solvents on the electroreduction of CO<sub>2</sub>: A comparison of theoretical approaches. *Physical Chemistry Chemical Physics* **2015**, *17*, 13949–13963.

- (64) Lespes, N.; Filhol, J. S. Using Implicit Solvent in Ab Initio Electrochemical Modeling: Investigating Li<sup>+</sup>/Li Electrochemistry at a Li/Solvent Interface. *Journal of Chemical Theory and Computation* **2015**, *11*, 3375–3382.
- (65) Deubel, D. V.; Lau, J. K.-c. In silico evolution of substrate selectivity : comparison of organometallic ruthenium complexes with the anticancer drug cisplatin . **2006**, *2*, 2451–2453.
- (66) Kua, J.; Thrush, K. L. HCN, Formamidic Acid, and Formamide in Aqueous Solution: A Free-Energy Map. *J. Phys. Chem. B* **2016**, *120*, 8175–8185.
- (67) Nørskov, J. K.; Rossmeisl, J.; Logadottir, A.; Lindqvist, L.; Kitchin, J. R.; Bligaard, T.; Jonsson, H. Origin of the overpotential for oxygen reduction at a fuel-cell cathode. *The Journal of Physical Chemistry B* **2004**, *108*, 17886–17892.
- (68) Curutchet, A.; Colinet, P.; Michel, C.; Steinmann, S. N.; Le Bahers, T. Two-sites are better than one: revisiting the OER mechanism on CoOOH by DFT with electrode polarization. *Physical Chemistry Chemical Physics* **2020**, *22*, 7031–7038.
- (69) Tsai, C.; Chan, K.; Nørskov, J. K.; Abild-Pedersen, F. Rational design of MoS<sub>2</sub> catalysts: tuning the structure and activity via transition metal doping. *Catalysis Science & Technology* **2015**, *5*, 246–253.
- (70) Tsai, C.; Chan, K.; Nørskov, J. K.; Abild-Pedersen, F. Theoretical insights into the hydrogen evolution activity of layered transition metal dichalcogenides. *Surface Science* **2015**, *640*, 133–140.
- (71) Kibsgaard, J.; Tsai, C.; Chan, K.; Benck, J. D.; Nørskov, J. K.; Abild-Pedersen, F.; Jaramillo, T. F. Designing an improved transition metal phosphide catalyst for hydrogen evolution using experimental and theoretical trends. *Energy & Environmental Science* **2015**, *8*, 3022–3029.

# Graphical TOC Entry

